

The moment duration scaling relation for slow rupture arises from transient rupture speeds

Kjetil Thøgersen^{1,2*}, Henrik Andersen Sveinsson^{1,3}, Julien Scheibert⁴, François Renard^{1,2,5}, Anders Malthe-Sørenssen^{1,3}

¹Physics of Geological Processes, The NJORD Centre, University of Oslo, Norway

²Department of Geosciences, University of Oslo, Norway

³Department of Physics, University of Oslo, Norway

⁴Univ Lyon, Ecole Centrale de Lyon, ENISE, ENTPE, CNRS, Laboratoire de Tribologie et Dynamique des Systèmes LTDS, F-69134, Ecully, France

⁵University Grenoble Alpes, University Savoie Mont Blanc, CNRS, IRD, IFSTTAR, ISTerre, 38000

Grenoble, France

Key Points:

- A Burridge-Knopoff model with only two dimensionless parameters; the homogeneous stress on a fault and a velocity strengthening friction term.
- The simplicity of the model allows for both numerical and analytical calculations of moment versus duration scaling relationships during fault slip.
- Moment versus duration scaling relation for slow events arises from transient rupture speeds.

Plain language summary

Observations have shown that the duration of earthquakes is related to the seismic moment through a power law. The power law exponent is different for regular earthquakes and slow aseismic rupture, and the origin of this difference is currently debated in the literature. In this letter, we introduce a minimal mechanical friction model that contains both slow and regular earthquakes, and demonstrate that the different power laws emerge naturally within the model because the propagation speed of slow earthquakes decays as a power law in time whereas the propagation speed of regular earthquakes remains fairly constant.

*kjetil.thogersen@fys.uio.no

Abstract

28 The relation between seismic moment and earthquake duration for slow rupture fol-
 29 lows a different power law exponent than sub-shear rupture. The origin of this dif-
 30 ference in exponents remains unclear. Here, we introduce a minimal one-dimensional
 31 Burridge-Knopoff model which contains slow, sub-shear and super-shear rupture, and
 32 demonstrate that different power law exponents occur because the rupture speed of
 33 slow events contains long-lived transients. Our findings suggest that there exists a
 34 continuum of slip modes between the slow and fast slip end-members, but that the
 35 natural selection of stress on faults can cause less frequent events in the intermediate
 36 range. We find that slow events on one-dimensional faults follow $\bar{M}_{0,\text{slow},1D} \propto \bar{T}^{0.63}$
 37 with transition to $\bar{M}_{0,\text{slow},1D} \propto \bar{T}^{\frac{3}{2}}$ for longer systems or larger prestress, while the
 38 sub-shear events follow $\bar{M}_{0,\text{sub-shear},1D} \propto \bar{T}^2$. The model also predicts a super-shear
 39 scaling relation $\bar{M}_{0,\text{super-shear},1D} \propto \bar{T}^3$. Under the assumption of radial symmetry, the
 40 generalization to two-dimensional fault planes compares well with observations.
 41

1 Introduction

Over the last decades, an increasing number of slow slip events on faults have been reported (Bürgmann, 2018). A measure that is viewed as a key to unravelling the mechanism of slow and fast rupture is the relation between seismic moment M_0 and slip event duration T . Regular fast earthquakes have long been known to follow a moment duration scaling relation of $M_0 \propto T^3$. Ide et al. suggested that slow events follow a unified scaling relation $M_0 \propto T$ (Ide, Beroza, Shelly, & Uchide, 2007). They suggested that the linear relation between moment and duration for slow events can be explained in two ways: (1) the average slip is proportional to the fault length as for fast propagation, and the stress drop is constant for all events, which gives the relation $M_0 \propto T$. (2) the slip amount is constant for all events, and the fault area increases linearly with time $L^2 \propto T$, which results in $M_0 \propto T$. Peng and Gomberg (2010) elaborated on the ideas of Ide et al. (2007) and reached a different conclusion; that rupture should span a continuum between fast and slow velocity end-members. Later studies have reported on a variety of scalings between moment and duration ranging from $M_0 \propto T$ to $M_0 \propto T^2$ (Aguiar, Melbourne, & Scrivner, 2009; Frank, Rousset, Lasserre, & Campillo, 2018; Gao, Schmidt, & Weldon, 2012; Ide, Imanishi, Yoshida, Beroza, & Shelly, 2008).

The shape of slip patches can also influence the observed scaling. Ben-Zion (2012) argued that fractal slip patches can result in a scaling relation $M_0 \propto T^2 / \log(T)$ because the average displacement is approximately constant rather than proportional to the rupture dimension. Bounded propagation can also play an important role (Ben-Zion, 2012; Gomberg, Wech, Creager, Obara, & Agnew, 2016). Gomberg et al. (2016) suggested that the scaling relation between moment and duration is the same for slow and fast events, but that a transition occurs between a two-dimensional scaling and a one-dimensional scaling when the rupture propagation switches from unbounded to bounded in one direction. Assuming the fault displacement can be approximated using dislocation theory, this results in a transition from T^2 to T . They suggest that there should be a bimodal but continuous distribution of slip modes, and that a difference in scaling relations alone does not imply a fundamental difference between fast and slow slip. The above mentioned theoretical considerations implicitly assume constant rupture velocity. However, this contradicts observations by Gao et al. (2012) that show that the average rupture speed for slow events decreases with increasing seismic moment, which is a strong indication of transient rupture speeds.

Slow slip events emerge in numerical models with rate-and-state friction. Colella, Dieterich, and Richards-Dinger (2011) simulated a Cascadia-like subduction zone using rate-and-state friction. They analyzed a large number of slip events, and found that the seismic moment M_w scales as $M_w \propto T^{1.5}$ for $M_w \leq 5.6$ with a transition to $M_w \propto T^2$ for $M_w > 5.6$. Shibazaki, Obara, Matsuzawa, and Hirose (2012) modeled the subduction zone of southwest Japan with rate-and-state friction. For slow events, they found a scaling $M_0 \propto T^{1.3}$. Liu (2014) used rate-and-state friction on a 3D subduction fault model and found a scaling $M_0 \propto T^{1.85}$. Romanet, Bhat, Jolivet, and Madariaga (2018) highlighted the role of interactions between faults. They argue that the scaling relationships of slow slip events and earthquakes emerge from geometrical complexities due to interactions between fault segments. The moment duration scalings have not only been addressed using rate-and-state friction. Ide (2008) introduced a brownian walk model for slow rupture, where the assumption is that there is a random expansion and contraction of the fault area, so that its radius can be described as a Brownian walk with a damping term. This model predicts $M_0 \propto T$ for large T .

Here, our goal is to answer the following two questions: (1) Is there a separation of two distinct classes (Ide et al., 2007), or is there a continuum of possible scaling relations between the fast and slow end-members (Peng & Gomberg, 2010)? (2) Can a difference in $M_0 - T$ scaling relations alone be attributed to different physical mecha-

95 nisms behind slow and fast rupture? We address both (1) and (2) through a Burridge-
 96 Knopoff type model with Amontons-Coulomb friction with a velocity strengthening
 97 friction term that has previously been shown to contain a large variety of rupture
 98 phenomena, including sub-shear, super-shear and slow propagation (Thøgersen et al.,
 99 2019). Velocity strengthening friction has been shown to be a generic feature of dry
 100 friction (Bar-Sinai, Spatschek, Brener, & Bouchbinder, 2014), and has been reported
 101 in Halite shear zones at low slip speeds or large confining pressures (Shimamoto, 1986).
 102 The friction law can also be interpreted as a transition from a dry contact to a lubri-
 103 cated sliding regime with increasing velocity (a Stribeck curve) under the additional
 104 assumption that the transition from dry to contact to lubricated sliding occurs at a
 105 small sliding speed (Gelinck & Schipper, 2000; Olsson, Åström, De Wit, Gäfvert, &
 106 Lischinsky, 1998).

107 For homogeneously stressed faults, the model can be reduced to only two dimen-
 108 sionless parameters $\bar{\tau}$ and $\bar{\alpha}$ representing the prestress and a velocity strengthening
 109 friction term, respectively. The advantage of such approach is that the simplicity of the
 110 model allows us to calculate moment duration scaling relations both through numer-
 111 ical simulations and through analytical calculations. Through numerical simulations,
 112 we demonstrate that there exists a continuum of rupture modes between the slow
 113 and fast end-members, but that the most likely selection of $\bar{\tau}$ in nature produces two
 114 distinct classes separating sub-shear and slow rupture velocities. Through analytical
 115 calculations, we show that the scaling relation for slow fronts arises due to long-lived
 116 transients in the rupture velocity. Such transient rupture velocity has been observed
 117 in nature through a dependence on the average rupture speed on the seismic moment
 118 for slow fronts (Gao et al., 2012). In addition, the model predicts a separate scaling
 119 for super-shear rupture not previously reported in the literature.

120 **2 A one-dimensional Burridge-Knopoff containing slow and fast rup-** 121 **ture**

122 We solve the one-dimensional Burridge-Knopoff model (Burridge & Knopoff,
 123 1967) with Amontons-Coulomb friction with a linear velocity strengthening term. The
 124 dimensionless equation of motion for a chain of N blocks can be written as (a detailed
 125 derivation can be found in the supplementary information)

$$\ddot{\bar{u}}_i - \bar{u}_{i-1} - \bar{u}_{i+1} + 2\bar{u}_i + \bar{\alpha}\dot{\bar{u}}_i - \bar{\tau}^\pm = 0, \quad \forall i \in [0, N], \quad (1)$$

126 where \bar{u} is the dimensionless displacement

$$\bar{\tau}^\pm = \frac{\tau/\sigma_N \mp \mu_k}{\mu_s - \mu_k} \quad (2)$$

127 is the dimensionless prestress where σ_N is the normal stress, τ is the initial shear
 128 stress, and μ_s and μ_k are the static and dynamic coefficients of friction, respectively.
 129 \pm denotes the sign of the block velocity. For positive velocities, we only need to
 130 consider $\bar{\tau}^+$, but negative velocities can occur in a small subset of our simulations. In
 131 such situations, we need to prescribe the relation between μ_s and μ_k , which we set to
 132 $\mu_s = 2\mu_k$, so that $\bar{\tau}^- = \bar{\tau}^+ + 2$. In the rest of the paper we will use $\bar{\tau}$ as a reference
 133 to $\bar{\tau}^+$. The second dimensionless parameter

$$\bar{\alpha} = \frac{\alpha}{\sqrt{\rho E}} \quad (3)$$

134 is a viscous term, where ρ is the density, E is the elastic modulus, and α is a velocity
 135 strengthening term with units [Pa s/m]. $\bar{\alpha}$ can range from 0 to infinity, where $\bar{\alpha} = 0$ re-
 136 covers the ordinary Amontons-Coulomb friction without viscosity. $\bar{\tau}$ has an upper limit
 137 of 1, where the prestress equals the static friction threshold. For $\bar{\tau} < 0$, steady state
 138 propagation does not occur (Amundsen et al., 2015). This corresponds to a prestress

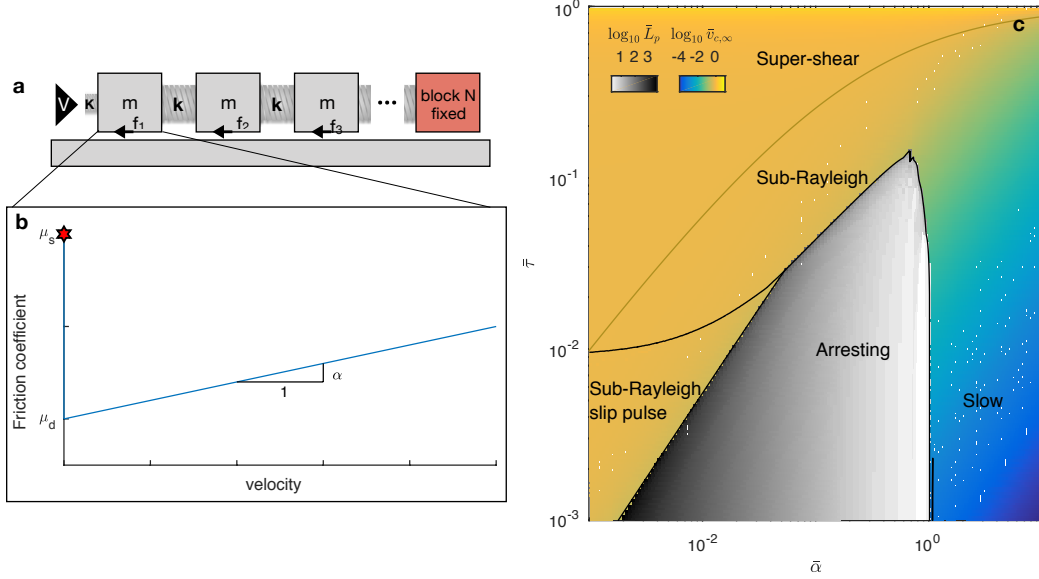


Figure 1. (a) We solve the one-dimensional Burridge-Knopoff model with Amontons-Coulomb friction with velocity-strengthening dynamic friction for homogeneously loaded faults. V is the driving velocity, K is the driving spring constant, m is the block mass, k is the spring constant, and f_i is the friction force on block i . The friction law is given by a static friction coefficient μ_s , and a dynamic friction coefficient μ_d plus a velocity strengthening term αv (b). To obtain the seismic moment and duration for a given fault length we fix the block at position N . The model can be written in dimensionless units with only two parameters: $\bar{\tau}$ representing the prestress on the fault, and $\bar{\alpha}$ representing the velocity strengthening friction term. This simple model produces a large variety of slip, including, slip pulses, cracks, sub-Rayleigh rupture, super-shear rupture, slow rupture, and arresting fronts (c). The colorbars show the rupture length \bar{L} of arresting fronts, and the steady state rupture speed $\bar{v}_{c,\infty}$ for given $\bar{\tau}$ and $\bar{\alpha}$ (adapted from Thøgersen et al. (2019))

139 below the dynamic friction level. We thus simulate $\bar{\tau} \in [10^{-7}, 1]$ and $\bar{\alpha} \in [10^{-3}, 10]$.
 140 The boundary conditions assuming triggering through soft tangential loading (small
 141 driving velocity V and driving spring stiffness K) are given by $\bar{u}_{-1} = \bar{u}_0 + 1 - \bar{\tau}$. The
 142 rightmost block is fixed so that $\bar{u}_N = 0$. Blocks start to move once the static friction
 143 threshold is reached, which in dimensionless units can be written as

$$\bar{u}_{i-1} + \bar{u}_{i+1} - 2\bar{u}_i \geq 1 - \bar{\tau} \quad (4)$$

144 Moving blocks restick if the velocity changes sign. The system is sketched in Figure 1a.
 145 This model has previously been used to determine the steady state rupture velocity
 146 which includes sub-shear, supershear, and slow rupture, as well as an arresting region
 147 at low $\bar{\tau}$ and intermediate $\bar{\alpha}$ (Thøgersen et al., 2019). The steady state front speed
 148 $\bar{v}_{c,\infty}$ can be found exactly when $\bar{\alpha} = 0$ (Amundsen et al., 2015). For $\bar{\alpha} > 0$ we can use
 149 the empirical expression (Thøgersen et al., 2019)

$$\bar{v}_{c,\infty} \approx \frac{1 - e^{-\frac{\bar{\tau}}{\bar{\alpha}(1-\bar{\tau})}}}{\sqrt{1 - \bar{\tau}^2}}. \quad (5)$$

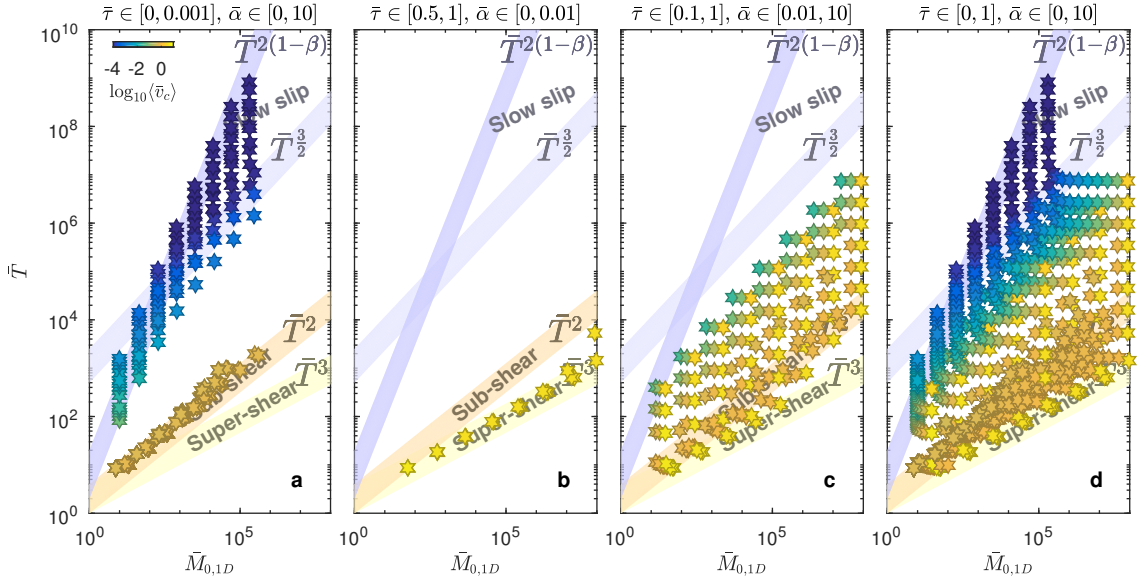


Figure 2. One-dimensional seismic moment $\bar{M}_{0,1D}$ and event duration \bar{T} obtained from simulations. The color of the markers show the average front speed $\langle \bar{v}_c \rangle$. The origin of the four different scaling exponents $\{2(1 - \beta), \frac{3}{2}, 2, 3\}$ is discussed in detail in the text. (a) In the limit of small $\bar{\tau}$, there is a separation in two distinct scalings for fast and slow events. (b) For large $\bar{\tau}$ the model predicts super-shear rupture, which has a different scaling exponent than regular sub-shear earthquakes. (c): For intermediate $\bar{\tau}$, the central part of the diagram is populated. (d) Results from the entire range of $\bar{\tau}$ and $\bar{\alpha}$ show that moment duration can exhibit a continuum of slip modes in between the slow and fast end-members.

3 Moment duration scaling relations

3.1 Model results

We run simulations until all blocks have ruptured or all blocks have stopped. We have performed 1120 simulations to obtain the moment duration diagram with $N \in 5 \times 2^{\{0,7\}}$. In dimensionless units the zeroth order moment for rupture propagation along a line is

$$\bar{M}_{0,1D} = \langle \bar{u} \rangle \bar{L}, \quad (6)$$

where $\langle \bar{u} \rangle$ is the average displacement on a fault of length \bar{L} . We run the simulations until all blocks are immobile, or until the average velocity reaches 0.1% of the steady state slip speed $\bar{\tau}/\bar{\alpha}$ (Thøgersen et al., 2019). The seismic moment and the duration are measured when 99% of the total displacement has been reached.

Figure 2 shows the measured $\bar{M}_{0,1D}$ and event duration \bar{T} for all simulations. If the stress drop is small compared to the absolute shear stress, as is often found for faults (Shearer, Prieto, & Hauksson, 2006), τ should often lie close to the dynamic level, which corresponds to $\bar{\tau} \simeq 0$. For low values of $\bar{\tau}$, the arresting region in $(\bar{\tau}, \bar{\alpha})$ gives rise to a separation of these scaling relations, so that fast and slow rupture fall into two distinct lines in the moment duration diagram (Figure 2a). This is in line with the ideas of Ide et al. (2007). This separation occurs because steady state propagation at small $\bar{\tau}$ and intermediate $\bar{\alpha}$ is forbidden (Figure 1a). If we include also larger prestress values we obtain a continuum of slip modes in the moment duration diagram (Figure 2d), in line with the suggestions of Peng and Gomberg (2010). The model also predicts a second scaling relations for super-shear rupture, which is found at large $\bar{\tau}$, that has not previously been reported (Figure 2b).

3.2 Origin of scaling relations - analytical calculations

The simplicity of the model allows an analytical treatment of several aspects which helps explain the various scaling relations between seismic moment and event duration. We summarize the analytical predictions for slip, front speed and event duration, and explain why the different scaling relations appear. A detailed derivation is given in the supplementary information.

First, we can determine the average slip on a fault. If the stress is at the dynamic level after rupture (the stress drop equals $\bar{\tau}$), we can calculate $\langle \bar{u} \rangle$ exactly

$$\langle \bar{u} \rangle = \frac{\bar{\tau} \bar{L}^2}{3} + \frac{(1 - \bar{\tau}) \bar{L}}{2}. \quad (7)$$

Equation 7 is derived for soft tangential loading, and we stress that a different boundary conditions could lead to different dependencies between \bar{L} , $\langle \bar{u} \rangle$ and $\bar{\tau}$. Combining equation 7 with equation 6 we find that the seismic moment can be written as

$$\bar{M}_{0,1D} = \frac{\bar{\tau} \bar{L}^3}{3} + \frac{(1 - \bar{\tau}) \bar{L}^2}{2}, \quad (8)$$

which only depends on the prestress $\bar{\tau}$ and the length of the fault \bar{L} . To obtain the moment duration scaling relation we need to determine $\bar{L}(\bar{T})$, and thus have to combine equation 8 with information about the rupture propagation and the afterslip (i.e. the amount of slip after the propagation has stopped).

A key observation on the rupture propagation is shown in Figure 3. While fast fronts exhibit short transients and quickly reach the steady state propagation speed given by equation 5, slow rupture contains long transients where the propagation speed decays. In the figure, we have illustrated this effect as a decay in the average rupture speed $\langle \bar{v}_c \rangle$ with increasing seismic moment \bar{M}_0 . This result is in line with observations by Gao et al. (2012).

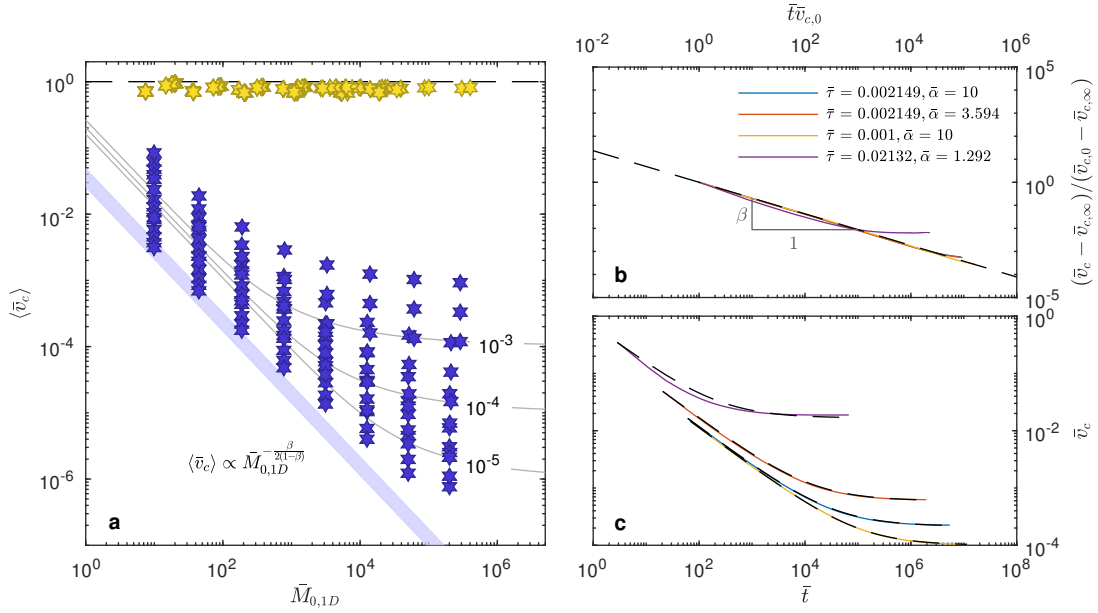


Figure 3. (a) Average propagation speed $\langle \bar{v}_c \rangle$ as a function of seismic moment for $\bar{\tau} \in [10^{-7}, 10^{-3}]$ and $\bar{\alpha} \in [10^{-3}, 10]$. Yellow markers show fast fronts while blue show slow fronts. Grey lines show predictions for $\bar{\alpha} = 10$ and $\bar{\tau} \in [10^{-5}, 10^{-3}]$ from equation 14. The prediction for $\bar{\tau} = 0$ follows $\langle \bar{v}_c \rangle \propto \bar{M}_{0,1D}^{-\frac{\beta}{2(1-\beta)}}$. (b) This transient velocity can be approximated by subtracting the steady state front velocity $v_{c,\infty}$ from equation 5 and scaling with the initial rupture velocity $v_{c,0}$ found from equation S32. The dashed line shows $(\bar{t}\bar{v}_{c,0})^{-\beta}$ with $\beta = 0.6852$. (c) The same fit when the steady state is not subtracted.

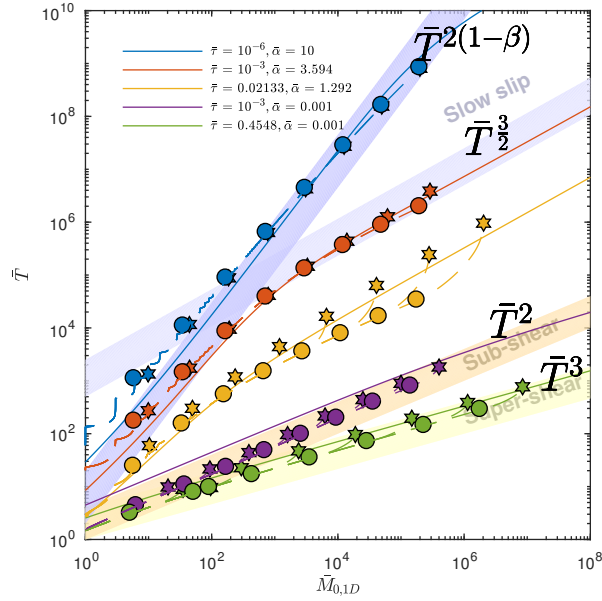


Figure 4. Moment duration scaling examples. Dashed lines show the evolution in time of the seismic moment. (star) shows the final value of the duration and the moment, while (circle) marks the point when the front reaches the end of the fault (i.e without afterslip) for $N = 5 \times 2^{\{0,7\}}$. The solid lines show the predictions of moment versus duration discussed in the text. The top three curves use the slow scaling (equation 17 and 18), while the bottom two use the fast scaling relation (equation 11). The colored regions highlight the different scaling exponents discussed in the text.

3.2.1 Fast regime

The short transients in the fast regime indicate that we can approximate the rupture length by

$$\bar{L} = \int_0^{\bar{t}_{\text{rupture}}} \bar{v}_c(t') dt' \approx \bar{v}_{c,\infty} \bar{t}_{\text{rupture}}, \quad (9)$$

where t_{rupture} is the time it takes for a rupture front to reach the end of the fault. The time it takes to arrest completely depends upon the existence of a backward propagating arresting front. If we assume that this backward propagation occurs at roughly the same speed as the forward propagation we obtain

$$\bar{T} \approx \frac{2\bar{L}}{\bar{v}_{c,\infty}} \quad (10)$$

so that

$$\bar{M}_{0,1D} \approx \frac{\bar{\tau}}{3} \left(\frac{\bar{v}_{c,\infty} \bar{T}}{2} \right)^3 + \frac{1-\bar{\tau}}{2} \left(\frac{\bar{v}_{c,\infty} \bar{T}}{2} \right)^2. \quad (11)$$

This relation implies that there is a separate scaling for sub-shear ($\bar{\tau} \rightarrow 0$) and super-shear rupture ($\bar{\tau} \rightarrow 1$) in our simulations:

$$\bar{M}_{0,\text{sub-shear},1D} \propto \bar{T}^2 \quad (12)$$

and

$$\bar{M}_{0,\text{super-shear},1D} \propto \bar{T}^3. \quad (13)$$

Note that we also predict that $\bar{M}_{0,\text{sub-shear},1D}$ will transition to a \bar{T}^3 scaling for large \bar{L} if $\bar{\tau}$ is small but nonzero. The moment duration, in the fast regime using equation 11, is shown in the two bottom lines of Figure 4. This figure also shows numerically obtained values for the moment duration. The agreement between the numerical simulations and equation 11 is good.

3.2.2 Slow regime

For slow fronts, $\bar{v}_c(\bar{t})$ is transient. To obtain an approximation for $\bar{v}_c(\bar{t}, \bar{\alpha}, \bar{\tau})$, we plot $\bar{v}_c(\bar{t})$ for a selection of $\bar{\tau}$ and $\bar{\alpha}$ in Figure 3. All curves collapse when we subtract the steady state front velocity $v_{c,\infty}$ and scale with the initial rupture velocity $v_{c,0}$ given in equation S32. We can then write down

$$\bar{v}_{c,\text{slow}} \approx (\bar{v}_{c,0} - \bar{v}_{c,\infty})(\bar{v}_{c,0} \bar{t})^{-\beta} + \bar{v}_{c,\infty} \quad (14)$$

Figure 3 shows that this relation fits well with simulations for small $\bar{\tau}$, and we measure empirically the exponent $\beta \approx 0.6852$. To obtain a parametric equation for \bar{M}_0 and \bar{T} , we need to find $\bar{T}(\bar{L})$. \bar{T} has two main components; the time it takes to rupture a fault of length \bar{L} , \bar{t}_{rupture} , and the time it takes for all motion to stop. Unlike for fast fronts, the arresting phase in the slow regime is not governed by a backward propagating arresting front, but rather a slow exponential decay in velocity. We denote this time $\bar{t}_{\text{afterslip}}$, and define

$$\bar{T} = \bar{t}_{\text{rupture}} + \bar{t}_{\text{afterslip}}. \quad (15)$$

\bar{t}_{rupture} can be found from equation 14

$$\bar{L} = \int_0^{\bar{t}_{\text{rupture}}} \bar{v}_c(\bar{t}') d\bar{t}' \quad (16)$$

$$= \frac{(\bar{v}_{c,0} - \bar{v}_{c,\infty})}{(1-\beta)\bar{v}_{c,0}^\beta} \bar{t}_{\text{rupture}}^{1-\beta} + \bar{v}_{c,\infty} \bar{t}_{\text{rupture}}, \quad (17)$$

The afterslip time can also be found analytically, and the detailed calculation is given in the supplementary information. The result is

$$\bar{t}_{\text{afterslip}} = \log(100) \frac{2\bar{L}^2 \bar{\alpha}}{\pi^2} \quad (18)$$

224 where $\log(100)$ indicates that we take the time when 99% of the slip has been ac-
 225 cumulated (which is necessary because the afterslip is exponentially decaying). The
 226 prediction of seismic moment versus duration can then be found using equation 8 for
 227 the seismic moment, equation 17 for \bar{t}_{rupture} (this has to be solved numerically for
 228 nonzero $\bar{\tau}$), and equation 18 for $\bar{t}_{\text{afterslip}}$, with $\bar{T} = \bar{t}_{\text{rupture}} + \bar{t}_{\text{afterslip}}$. The excellent
 229 agreement between the analytical approach and the numerical simulations is demon-
 230 strated in Figure 4.

231 We can determine the bound on the slow front scaling relation by noting that
 232 for infinitesimal $\bar{\tau}$, $\bar{v}_{c,\infty} \approx 0$ and $\bar{M}_{0,1D} \approx \frac{\bar{L}^2}{2}$. This yields

$$\bar{T}_{\bar{\tau}=0} = \bar{v}_{c,0}(1 - \beta)^{\frac{1}{1-\beta}} \bar{L}^{\frac{1}{1-\beta}} + \log(100) \frac{2\bar{L}^2\bar{\alpha}}{\pi^2}, \quad (19)$$

233 where the first term will dominate over the second term (negligible afterslip) for large
 234 \bar{L} because $\frac{1}{1-\beta} > 2$ for the measured $\beta = 0.6852$. We can then solve for

$$\bar{L} \approx \frac{\bar{T}_{\bar{\tau}=0}^{1-\beta}}{(1 - \beta)\bar{v}_{c,0}^{1-\beta}} \quad (20)$$

235 which gives us

$$\bar{M}_{0,\text{slow},1D,\bar{\tau}=0} \approx \frac{\bar{L}^2}{2} \propto \bar{T}^{2(1-\beta)} \quad (21)$$

236 with $2(1 - \beta) \approx 0.6296$. We also observe a transition to a different scaling at large
 237 $\bar{M}_{0,1D}$ when $\bar{\tau}$ is nonzero. To obtain the exponent in this regime, we note that in this
 238 limit the steady state rupture velocity is reached, so that

$$\bar{T} \approx \frac{\bar{L}}{\bar{v}_{c,\infty}} + \log(100) \frac{2\bar{L}^2\bar{\alpha}}{\pi^2}. \quad (22)$$

239 For large \bar{L} and nonzero $\bar{\tau}$, the afterslip will dominate, so that $\bar{L} \propto \bar{T}^{\frac{1}{2}}$. The cubic
 240 term in equation 8 will eventually dominate, which results in

$$\bar{M}_{0,\text{slow},1D,\bar{L} \gg 1, \bar{\tau} > 0} \propto \bar{T}^{\frac{3}{2}} \quad (23)$$

241 This means that the moment duration scaling relation in the slow regime is expected
 242 to follow a power law with exponent $2(1 - \beta)$ with a possible transition to $\frac{3}{2}$ at large
 243 $\bar{M}_{0,1D}$

244 4 Discussion

245 We have demonstrated that a simple Burridge-Knopoff model with Amontons-
 246 Coulomb friction is capable of reproducing the range of power law scaling relations
 247 between seismic moment and duration observed in nature. The simplicity of the model
 248 means that we can calculate the scaling relations analytically, and we find the one-
 249 dimensional exponents $2(1 - \beta)$ with a transition to $\frac{3}{2}$ for large seismic moments for
 250 slow rupture, 2 for sub-shear rupture, and 3 for super-shear rupture, where β is the
 251 power law exponent of the transient slow rupture velocity.

252 In this letter, we aimed to address two questions. First, whether there is a separa-
 253 tion of two distinct classes, or is there a continuum of possible scaling relations
 254 between the fast and slow end-members. We argue that the most likely value for $\bar{\tau}$ is
 255 close to 0, which corresponds to shear stress at the dynamic level, or to ruptures where
 256 the stress drop is small compared to the background stress like in faults (Shearer et
 257 al., 2006). If this is indeed the case, the moment duration scaling should contain a
 258 continuum of slip modes between the slow and fast end-members. However, because
 259 large $\bar{\tau}$ would in this case be unlikely, it would result in a distinction of fast and slow

260 scalings simply because this is more likely. This would indicate that both the interpre-
 261 tations by Ide et al. (2007) and by Peng and Gomberg (2010) hold in the sense that
 262 there is a continuum of slip modes, but the natural variation of $\bar{\tau}$ could result in more
 263 frequent events along the end-member scalings.

264 In our simulations, the separation into the slow and sub-shear scaling relations
 265 occurs spontaneously under the assumption that $\bar{\tau} \approx 0$. It has also been suggested that
 266 the observed separation could be strongly affected by instrumental limitations (Agnew,
 267 2009). In particular because the vastly different time-scales involved in aseismic and
 268 sub-shear rupture require different measurement techniques (Gomberg et al., 2016;
 269 Peng & Gomberg, 2010).

270 The second question we aimed to address was whether a difference in $M_0 - T$
 271 scaling relations alone could be attributed to different physical mechanisms behind
 272 slow and fast rupture. Our model contains only two dimensionless parameters, which
 273 highlights that the observed scaling relations do not necessitate complex underlying
 274 mechanisms. The same friction law with different values for the coefficients and a
 275 varying prestress can explain the entire range of scaling relations, and the slow scaling
 276 regime arises simply because slow rupture speeds are transient. Our findings thus
 277 suggest that there could be a separation in slow and fast scalings without a difference
 278 in physical mechanism. To assign different physical mechanisms to slow and fast
 279 rupture thus requires more observations than a different scaling relation alone.

280 To compare our results to observations on faults, it is instructive to discuss
 281 relations that would be obtained for rupture on a 2D plane. If we can assume radial
 282 symmetry, we can use the same expression for $\langle \bar{u} \rangle$ as in 1D, but $\bar{M}_{0,2D} = \langle \bar{u} \rangle \bar{L}^2$, which
 283 changes the scaling by a term \bar{L} . This changes the scaling relations to

$$\bar{M}_{0,\text{sub-shear},2D} \propto \bar{T}^3 \quad (24)$$

$$\bar{M}_{0,\text{super-shear},2D} \propto \bar{T}^4 \quad (25)$$

$$\bar{M}_{0,\text{slow},2D} \propto \bar{T}^{\{3(1-\beta),2\}} \quad (26)$$

286 where $3(1 - \beta) \approx 0.9444$ is the exponent that is dominant for $\bar{\tau} = 0$ at large \bar{L} . This is
 287 remarkably close to the hypothesized exponent of 1 from observations (Ide et al., 2007).
 288 The transition from $3(1 - \beta)$ to 2 also indicates that a simple linear scaling relation
 289 between seismic moment and duration for slow events is not appropriate, because it is
 290 only valid at $\bar{\tau} = 0$. We find it likely that a scaling in the approximate range $M_0 \propto T$
 291 to T^2 should be observed for slow events, depending also on the decaying exponent
 292 β . For a constant $\bar{\alpha}$, this variation in the power law exponent occurs due to changes
 293 in the stress state of the interface. This is in line with observations, where different
 294 studies have reported on scaling exponents ranging from approximately 1 to 2 (Aguiar
 295 et al., 2009; Frank et al., 2018; Gao et al., 2012; Ide et al., 2007, 2008).

296 From our results in Figure 3 we are in a position to explain the observed relation
 297 between average rupture speed and seismic moment (Gao et al., 2012). A transient
 298 rupture speed with a decaying exponent β would result in a two-dimensional scaling
 299 relation $\langle \bar{v}_c \rangle \propto \bar{M}_0^{-\frac{\beta}{3(1-\beta)}}$. Gao et al. (2012) observed that slow events follow the
 300 approximate relation $\langle \bar{v}_c \rangle \propto \bar{M}_0^{-0.5 \pm 0.05}$, which indicates that $\beta \approx 0.6 \pm 0.025$. Using
 301 equation 26 yields a moment duration scaling relation for slow rupture following $\bar{M}_0 \propto$
 302 $\bar{T}^{\{1,1,1,3\}}$, which is fully consistent with their observed linear relationship between
 303 seismic moment and duration.

304 Here, we have assumed that propagation is not bounded. Gomberg et al. (2016)
 305 demonstrated that there will be a change from a two-dimensional scaling to a one-
 306 dimensional scaling when the rupture propagation goes from unbounded to bounded in
 307 one of the directions. While we have demonstrated that different scalings can originate
 308 without such effect, a bounded system would add a number of possible transitions in

309 moment duration, and would in principle allow for scaling relations following both the
 310 two-dimensional and the one-dimensional exponents.

311 5 Conclusion

312 Linear elasticity and Amontons-Coulomb friction with a viscous term is sufficient
 313 to produce a large variety in scaling exponents between seismic moment and duration.
 314 This suggests that different scaling relations for fast and slow slip events do not require
 315 different or complex underlying physical mechanisms. Our findings also suggest that
 316 there exists a continuum of slip modes between the slow and fast slip end-members,
 317 but that the natural selection of stress on faults can cause less frequent events in
 318 the intermediate range. We find that the sub-shear scaling follows $M_0 \propto T^2$ (which
 319 corresponds to T^3 in 2D), while the slow scaling follows $T^{2(1-\beta)}$ (which corresponds to
 320 $T^{3(1-\beta)}$ in 2D) with a transition to $T^{\frac{3}{2}}$ (T^2 in 2D) for larger seismic moments depending
 321 on the prestress. $\beta \approx 0.6852$ corresponds to the power law decay in the slow rupture
 322 velocity with time. The model also predicts a separate scaling for super-shear rupture
 323 with $M_0 \propto T^3$ (T^4 in 2D).

324 Acknowledgements

325 We thank David Morgan, Agnès Helmstetter, Michel Bouchon and Yehuda Ben-
 326 Zion for providing useful suggestions. K.T acknowledges support from EarthFlows -
 327 A strategic research initiative by The Faculty of Mathematics and Natural Sciences
 328 at the University of Oslo. H.A.S acknowledges support from the Research Council of
 329 Norway through the FRINATEK program, grant number 231621. Code to generate
 330 the data used for the figures in the manuscript is available on Github (Thøgersen,
 331 2019).

332 References

- 333 Agnew, D. (2009). Instrumental, theoretical, temporal, and statistical challenges in
 334 the search for transient deformations. In *Agu fall meeting abstracts*.
- 335 Aguiar, A. C., Melbourne, T. I., & Scrivner, C. W. (2009). Moment release rate
 336 of cascadia tremor constrained by gps. *Journal of Geophysical Research: Solid*
 337 *Earth*, *114*(B7).
- 338 Amundsen, D. S., Trømborg, J. K., Thøgersen, K., Katzav, E., Malthe-Sørenssen,
 339 A., & Scheibert, J. (2015). Steady-state propagation speed of rupture fronts
 340 along one-dimensional frictional interfaces. *Physical Review E*, *92*(3), 032406.
- 341 Bar-Sinai, Y., Spatschek, R., Brener, E. A., & Bouchbinder, E. (2014). On the
 342 velocity-strengthening behavior of dry friction. *Journal of Geophysical Re-*
 343 *search: Solid Earth*, *119*(3), 1738–1748.
- 344 Ben-Zion, Y. (2012). Episodic tremor and slip on a frictional interface with criti-
 345 cal zero weakening in elastic solid. *Geophysical Journal International*, *189*(2),
 346 1159–1168.
- 347 Bürgmann, R. (2018). The geophysics, geology and mechanics of slow fault slip.
 348 *Earth and Planetary Science Letters*, *495*, 112–134.
- 349 Burridge, R., & Knopoff, L. (1967). Model and theoretical seismicity. *Bulletin of the*
 350 *seismological society of america*, *57*(3), 341–371.
- 351 Colella, H. V., Dieterich, J. H., & Richards-Dinger, K. B. (2011). Multi-event simu-
 352 lations of slow slip events for a cascadia-like subduction zone. *Geophysical Re-*
 353 *search Letters*, *38*(16).
- 354 Frank, W. B., Rousset, B., Lasserre, C., & Campillo, M. (2018). Revealing the clus-
 355 ter of slow transients behind a large slow slip event. *Science advances*, *4*(5),
 356 eaat0661.
- 357 Gao, H., Schmidt, D. A., & Weldon, R. J. (2012). Scaling relationships of source pa-

- rameters for slow slip events. *Bulletin of the Seismological Society of America*, 102(1), 352–360.
- Gelinck, E., & Schipper, D. J. (2000). Calculation of stribeck curves for line contacts. *Tribology International*, 33(3-4), 175–181.
- Gomberg, J., Wech, A., Creager, K., Obara, K., & Agnew, D. (2016). Reconsidering earthquake scaling. *Geophysical Research Letters*, 43(12), 6243–6251.
- Ide, S. (2008). A brownian walk model for slow earthquakes. *Geophysical Research Letters*, 35(17).
- Ide, S., Beroza, G. C., Shelly, D. R., & Uchide, T. (2007). A scaling law for slow earthquakes. *Nature*, 447(7140), 76.
- Ide, S., Imanishi, K., Yoshida, Y., Beroza, G. C., & Shelly, D. R. (2008). Bridging the gap between seismically and geodetically detected slow earthquakes. *Geophysical Research Letters*, 35(10).
- Liu, Y. (2014). Source scaling relations and along-strike segmentation of slow slip events in a 3-d subduction fault model. *Journal of Geophysical Research: Solid Earth*, 119(8), 6512–6533.
- Olsson, H., Åström, K. J., De Wit, C. C., Gäfvert, M., & Lischinsky, P. (1998). Friction models and friction compensation. *Eur. J. Control*, 4(3), 176–195.
- Peng, Z., & Gomberg, J. (2010). An integrated perspective of the continuum between earthquakes and slow-slip phenomena. *Nature geoscience*, 3(9), 599.
- Romanet, P., Bhat, H. S., Jolivet, R., & Madariaga, R. (2018). Fast and slow slip events emerge due to fault geometrical complexity. *Geophysical Research Letters*, 45(10), 4809–4819.
- Shearer, P. M., Prieto, G. A., & Hauksson, E. (2006). Comprehensive analysis of earthquake source spectra in southern california. *Journal of Geophysical Research: Solid Earth*, 111(B6).
- Shibazaki, B., Obara, K., Matsuzawa, T., & Hirose, H. (2012). Modeling of slow slip events along the deep subduction zone in the kii peninsula and tokai regions, southwest japan. *Journal of Geophysical Research: Solid Earth*, 117(B6).
- Shimamoto, T. (1986). Transition between frictional slip and ductile flow for halite shear zones at room temperature. *Science*, 231(4739), 711–714.
- Thøgersen, K. (2019). *One-dimensional burridge knopoff model*. <https://github.com/kjetilthogersen/1dBurridgeKnopoffMatlab>. GitHub.
- Thøgersen, K., Sveinsson, H. A., Amundsen, D. S., Scheibert, J., Malthé-Sørensen, A., & Renard, F. (2019). A minimal model for slow, sub-rayleigh, super-shear and unsteady rupture propagation along homogeneously loaded frictional interfaces. *arXiv:1906.06079*.